JOURNAL OF MATERIALS SCIENCE 21 (1986) 3759–3766

Studies on spinodal decomposition in Cu–27Ni–2Cr alloy

P. PRASAD RAO
Department of Metallurgical Engineering, Karnataka Regional Engineering College, Surathkal, PO Srinivasnagar – 574157 (DK), Karnataka, India

B. K. AGRAWAL, A. M. RAO
Department of Metallurgical Engineering, Indian Institute of Technology, Bombay 400 076, India

Transformation characteristics of a Cu–27Ni–2Cr alloy were studied on ageing in the temperature range of 773 to 1073 K, by means of X-ray diffraction and transmission electron microscopy. It was concluded from morphological features that the alloy undergoes spinodal decomposition and the coherent spinodal was estimated to be 946 K. Yield stress increment on ageing was found to follow monotonically the strain amplitude and to be independent of the wavelength of composition modulation.

1. Introduction

The copper–nickel binary system is considered to be an ideal isomorphous system. However, the addition of a ternary alloying element such as iron, tin or chromium is known to introduce miscibility gaps which make these alloys susceptible to heat treatment. Cu–Ni–Fe alloys are widely used as magnetic materials. Cu–Ni–Sn alloys after appropriate heat treatment possess very high elastic limits which make them attractive as spring materials. Cu–Ni–Cr alloys find application as condenser tubes in marine atmospheres.

The miscibility gap in the Cu–Ni–Cr system was first reported by Meijering *et al.* [1]. They reported the existence of a miscibility gap consisting of two fcc phases which spread towards the Cu–Ni axis at decreasing temperatures. Investigations have been carried out on some Cu–Ni–Cr alloys in the composition range close to the copper-rich end of the miscibility gap with the primary aim of developing a substitute for the conventional 70 copper–30 nickel alloy with higher strength for applications in a marine atmosphere. These studies have led to considerable ambiguity regarding the nature of decomposition in alloys in this region of the miscibility gap. Wu and Thomas [2] and Chou *et al.* [3] in their electron microscopic studies observed many of the characteristics attributable to spinodal decomposition such as aligned precipitates, satellites in selected area diffraction patterns and absence of preferential precipitation at microstructural inhomogeneities like grain boundaries and dislocations. They therefore concluded that the alloys investigated by them decomposed by the spinodal mechanism. Bower *et al.* [4] also observed similar microstructural features in some alloys near the copper-rich end of the miscibility gap. They attributed these to artefacts and concluded that the alloys decomposed by a process of nucleation and growth. Knights and Wilkes [5] arrived at a similar conclusion after investigating a similar alloy. It should be noted that all the above mentioned workers based their conclusions solely on microstructural observations. It is known that microstructures similar to that of spinodal decomposition can also be obtained during precipitation by nucleation and growth mechanism [6]. Rao *et al.* [7] studied the transformations in a Cu–30 wt % Ni–5 wt % Cr alloy by X-ray diffraction techniques. The presence of sidebands on the X-ray diffraction profiles of the aged samples led them to conclude that the alloy decomposed by the spinodal mechanism. The composition of this alloy was just within the miscibility gap of the isothermal section at 1203 K of Cu–Ni–Cr ternary system as reported by Meijering *et al.* [1].

In the present work the transformation characteristics of a Cu–27 wt % Ni–2 wt % Cr alloy which lies just outside the miscibility gap have been investigated and correlated to microstructure and mechanical properties.

2. Experimental procedure

The alloy was prepared by melting electrolytic copper rods (99.96% purity), electrolytic grade nickel sheets (99.8% purity) and commercial purity 80–20 nichrome wire in the required proportion in an induction furnace. The chill cast ingots were homogenized in a silicon carbide furnace at 1373 K for 129.4 ksec. These were then sliced into strips of 10 mm × 25 mm × 100 mm and hot rolled to 2 mm thickness at 1273 K and then cold rolled to 1 mm thickness. All the experimental investigations were carried out on the samples cut out from this material.

Chemical analysis of the alloy was carried out by atomic absorption spectrophotometry. The analysis was found to be: Cr–1.9%; Ni–26.7%; and Cu–balance.

Heat treatments were carried out in a vertical Kanthal wound silica tubular furnace. The

0022–2461/86 $03.00 + .12

temperature was controlled within 2° C of the set point. All heat treatments were carried out in an atmosphere of flowing argon to minimize oxidation. The samples were solution treated at 1273 K for 900 sec and dropped into a bath of crushed ice and salt maintained at 260 K. These were subsequently aged over a range of temperatures for different lengths of time.

Hardness was measured on a Vickers hardness tester with a load of 10 kg. Tensile tests were carried out on samples of 15 mm gauge length at a strain rate of 1.39×10^{-3} sec^{-1} in a floor model Instron.

X-ray diffraction studies were carried out with a Philips diffractometer using a copper target and nickel filter. A scanning speed of 0.25° min^{-1} was employed. A scanning range of 3° on either side of the Bragg peak was found to be adequate to record both the side bands. All measurements were made on (2 0 0) profile as this peak affords the best combination of side band resolution and intensity.

Since each of these profiles is a combination of that due to α_1 and α_2 components of the X-radiation, the profiles were subjected to Rachinger analysis [8] to separate these two components. All the data from X-ray diffraction profiles reported in this work are those obtained from the α_1 component of the profile.

The samples for transmission electron microscopy were mechanically polished to 50 μm thickness using silicon carbide papers. These were then electropolished by the window technique using an electrolyte of nitric acid and methanol in the ratio 1 : 3 at 233 K and 18 V. The foils so obtained were studied in a Philips transmission electron microscope at 80 or 100 kV.

3. Results and discussion

3.1. X-ray diffraction studies

One of the most important characteristics of spinodal decomposition is the appearance of X-ray diffraction peaks with satellite lines. The location of side bands and their intensity give important information on the progress of transformation. Four isothermal ageing temperatures, 773, 823, 873 and 923 K, were selected for X-ray diffraction studies since the hardness studies revealed that the decomposition was fairly rapid at these temperatures.

Clearly identifiable side bands were observed on either side of the Bragg peak on the X-ray diffraction profiles of all the aged samples. During the initial periods of ageing the side bands were quite broad and spread over a large angular distribution of 0.45°. With increasing ageing time the intensity of the side band increased without any appreciable shift in its position. The increase in intensity was conspicuous in the central region of the broad side band. Peaks of the satellites on either side of the Bragg peak soon became clearly identifiable (Fig. 1). They continued to grow at the same angular position for some more ageing time. The side bands started to shift towards the Bragg peak after some more ageing time, which depended on the isothermal ageing temperature. During this period the side bands continued to increase in intensity on one hand and shift towards the Bragg peak on the other. After a long period of ageing the side bands had moved so close to the Bragg peak, they could no longer be distinguished as separate entities.

The wavelength of composition modulation was estimated from the X-ray diffraction data using the Daniel–Lipsom formula [9].

$$\lambda = \frac{ha_0 \tan \theta_B}{(\Delta\theta)(h^2 + k^2 + l^2)} \quad (1)$$

where $h\,k\,l$ are the Miller indices of the Bragg peak, θ_B is the Bragg angle, a_0 is the average lattice parameter, $\Delta\theta$ is the angular separation of side bands from the Bragg peak and λ is the wavelength of composition modulation.

Fig. 2 shows the variation of wavelength of composition modulation with ageing time at isothermal ageing temperature of 773, 823, 873 and 923 K on a log–log plot.

At a given isothermal ageing temperature the wavelength remained constant initially and started increasing after some ageing time. The initial constant wavelength λ_m increased with the increase of ageing temperature. λ_m values were 5.8, 6.2 and 8.4 nm at the ageing temperatures of 773, 823 and 873 K, respectively. The coarsening started earlier at higher ageing temperature. The coarsening commenced after 84, 11.4 and 5.4 ksec at the ageing temperatures of 773,

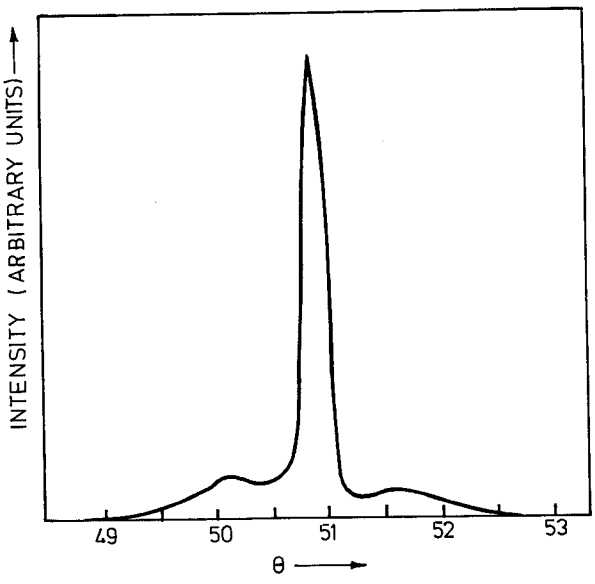

Figure 1 X-ray diffraction profile after ageing for 144 ksec at 823 K.

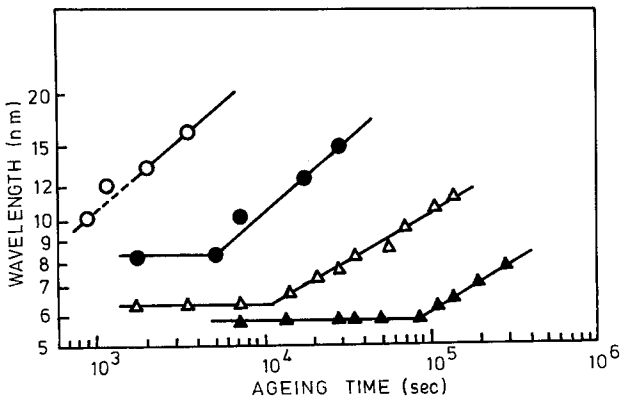

Figure 2 Variation of wavelength of composition modulation with ageing time at various ageing temperatures. (○) 923 K; (●) 873 K; (△) 823 K; (▲) 773 K.

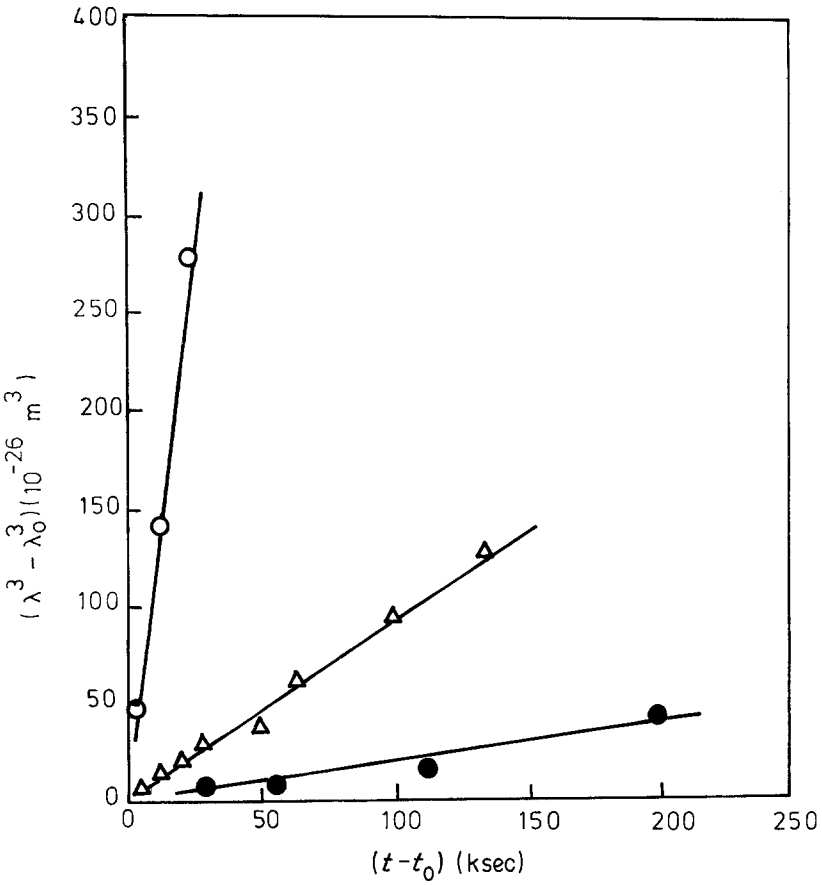

Figure 3 Plot of $\lambda^3 - \lambda_0^3$ against $t - t_0$ at various ageing temperatures. (○) 873 K; (△) 823 K; (●) 773 K.

823 and 873 K, respectively. No clearly identifiable λ_m could be observed at 923 K. It has therefore to be presumed that the coarsening must have started within 600 sec, which is the shortest ageing time used in the present work.

Cahn's [10] theory of spinodal decomposition predicts that there is a composition wave, with a wave number β_m, which has the maximum amplification factor and will be in a dominating position to grow as compared to the other waves. β_m does not change for short ageing durations. As ageing progresses and amplitude of the wave increases, the preferential growth of this wave keeps the wavelength constant. Such a constant wavelength has also been reported in a number of other systems [11–13].

The magnitude of this constant wavelength or wave number is dependent on the ageing temperature T and the following equation has been derived [14]

$$\beta_m^2 = (T - T_s^*)S''/4K \qquad (2)$$

where T_s^* is the coherent spinodal temperature, S'' is the second derivative of entropy with respect to composition and K is the gradient energy coefficient. It follows from this equation that as the ageing temperature is decreased β_m increases, i.e. λ_m decreases, which is exactly the observation in the present investigation.

The rate of increase of wavelength in the coarsening regime increased with the increase in the isothermal ageing temperature.

The data used in Fig. 2 has been reused in Fig. 3 to show the variation of λ with ageing time in the coarsening regime to fit into the following equation

$$\lambda^3 - \lambda_0^3 = k(t - t_0) \qquad (3)$$

where λ is the wavelength of composition modulation at time t, t_0 is the time at which coarsening starts and λ_0 is the initial constant wavelength. Linear plots were obtained at all the isothermal ageing temperatures indicating that Lifshitz–Slyozov [15] and Wagner [16] coarsening rule is obeyed which suggests that coarsening proceeds by a volume diffusion controlled mechanism.

It should be noted that for Ostwald ripening to be applicable, the coarsening of the precipitates must be occurring without any compositional change in the matrix and the precipitate. Butler and Thomas [17]

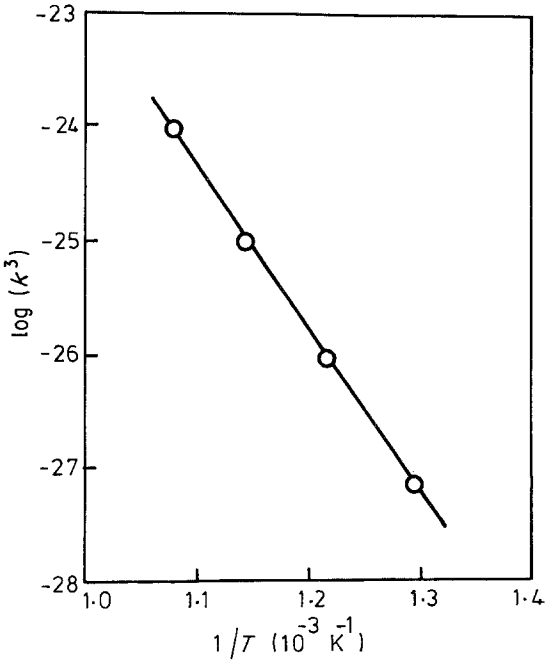

Figure 4 Plot of log (k^3) against $1/T$.

have found $t^{1/3}$ law to be obeyed during coarsening of spinodal Cu–Ni–Fe alloys. They observed that the amplitude remained constant during coarsening implying that the coexisting phases did not change their composition during coarsening. However in the investigations on a Ni–Cu–Si alloy by Miyazaki *et al.* [18] $t^{1/3}$ law was not observed. In that work the amplitude was found to increase even during coarsening suggesting that compositional adjustment was taking place between the precipitate and matrix. It will be shown later that in the alloy investigated in the present work, the amplitude had reached the maximum and remained so during coarsening. Since coarsening took place apparently under conditions of no compositional change, first criterion for Lifshitz–Slyozov–Wagner coarsening rule to be applicable is fulfilled.

The rate constants, k, determined from the slopes of the linear plots in Fig. 3 at various ageing temperatures T: 773; 823; 873; and also for 923 K which is not shown in Fig. 3 are plotted in Fig. 4 as k^3 against $1/T$. This again is a straight line indicating that the Lifshitz–Slyozov–Wagner coarsening rule is obeyed.

In Wagner's [16] formulation the constant k is given by

$$k = \left(\frac{8\gamma D C_0 V_m^2}{9RT}\right)^{1/3} \quad (4)$$

where γ is the particle matrix interfacial energy, D is the coefficient of diffusion of the solute in the matrix, C_0 is the solubility of the solute in equilibrium with a particle of infinite radius, V_m is the molar volume of the precipitate, R is the universal gas constant and T is the temperature. This shows that a plot of log k^3 against $1/T$ gives an activation energy for diffusion of solute in the matrix.

The activation energy as determined from the slope of the curve in Fig. 4 is 277.83 kJ mol^{-1}. Activation energy for diffusion in Cu–Ni system [19] is found to be of the same order as estimated here.

The two phases γ_1 and γ_2 formed as a result of spinodal decomposition of γ are rich in copper and nickel respectively. Saunderson *et al.* [20] have analysed the coarsened precipitates in a series of Cu–Ni–Cr alloys after ageing for very long periods at 923 K. Their analysis showed that γ_1 phase was depleted in nickel and chromium while γ_2 was depleted in copper. A Cu–34Ni–4Cr alloy after decomposition was found to have γ_1 phase of composition 71Cu–27Ni–2Cr and γ_2 of composition of 27Cu–63Ni–10Cr. Since considerable diffusion of nickel should take place away from γ_1 phase during its coarsening, the coarsening kinetics should depend on diffusion kinetics. This agrees well with the fact that activation energy for coarsening as estimated in this work compares well with that for diffusion of nickel in copper.

The activation energy was also calculated using the reaction rate theory by employing Arrhenius type equation [21]

$$S_1 = At \exp(-Q/RT) \quad (5)$$

where T is the temperature of isothermal transformation, t is the time, S_1 is the fraction transformed at time t, Q is the activation energy and A is a constant.

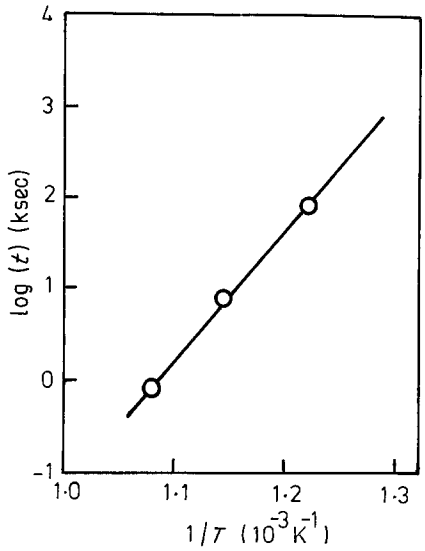

Figure 5 Plot of log t against $1/T$.

Volume fraction S_1 is taken as fixed wavelength, 10 nm. The time to transform to this wavelength is plotted against reciprocal of absolute temperature in Fig. 5. Activation energy calculated from the slope of the straight line was obtained as 273.09 kJ mol^{-1} which agrees well with the earlier theory. Reaction rate theory assumes that reactants have to surmount an energy barrier to form the low energy configuration. For the spinodal transformation there is no such barrier. The only barrier is that of diffusion. Therefore the activation energy as determined from the reaction rate theory should be interpreted as that for diffusion in these alloys. As already mentioned, activation energy compares well with that for diffusion in Cu–Ni system.

The coherent spinodal temperature for the alloy can be estimated from a knowledge of the initial constant wavelength. In Equation 2 if negligible temperature dependence is assumed for S'', then β_m^2 can be expected to be linear with respect to the ageing temperature T. A plot of β_m^2 against ageing temperature is shown in Fig. 6. The data for this are taken from Fig. 2. The plot shows a linear relationship between β_m^2 and T. The coherent spinodal temperature is obtained at 946 K by extrapolating the curve to intersect the x-axis.

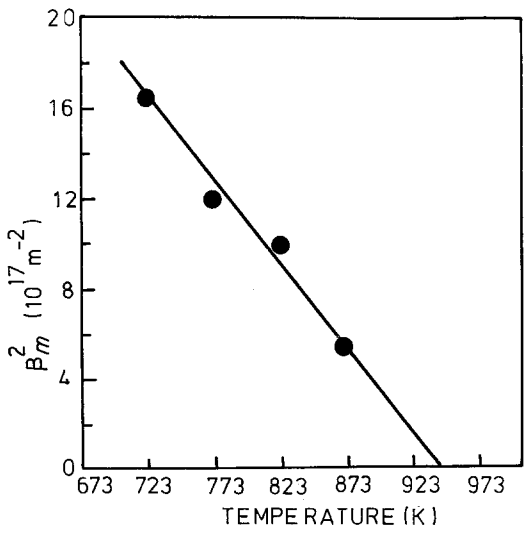

Figure 6 Plot of β_m^2 against ageing temperature.

Ditchek and Schwartz [22] have developed a model to obtain a measure of the concentration amplitude from integrated intensity of the side bands which takes into account the change of the sinusoidal modulation at the beginning of the ageing into a square wave modulation during the course of ageing. The ratio of the integrated intensity of the side band to that of the main Bragg peak is expressed as

$$R_{+}^{1/2} + R_{-}^{1/2} = \frac{2J_1(g\lambda\varepsilon s)}{J_0(g\lambda\varepsilon s)} \quad (6)$$

where $R_{+(-)}$ is the ratio of integrated intensity of side band on high (low) angle side to that of the Bragg peak, J_1 and J_0 are Bessel functions of first and zeroth order, respectively, ε is the strain amplitude, s is the scattering factor and g takes values from 1 for a sinusoidal modulation to $4/\pi$ for a square wave. R values were calculated by estimating the area under the Bragg peak and side bands using a planimeter. The side bands always merged with the Bragg peak without reaching zero intensity. Therefore it was assumed that the intensity of the side bands decreased linearly from their peak value to zero at the position of the Bragg angle. The value of $(g\lambda\varepsilon s)$ in Equation 6 was then obtained by solving the equation graphically. Complete details of estimating ε are given elsewhere [23].

Fig. 7 shows the variation of strain amplitude with ageing time at 773 K. On the same plot is also shown the variation of wavelength with ageing time. The third curve showing increment in yield stress will be discussed later. The strain amplitude is 0.004 to start with. With progressive ageing the strain amplitude increases continuously and reaches a peak value at 0.0065. Thereafter the strain amplitude remains a constant for further ageing. By comparing the two curves for ε and λ, it can be seen that the strain amplitude increases when the wavelength remains constant and remains stationary at the peak value when wavelength increases. This would imply that coarsening starts when phases have reached their equilibrium values.

Composition amplitude can be obtained from the strain amplitude, as the relation between them is quite direct as given by the following equation [24]

$$\varepsilon = \left(\frac{C_{11} + 2C_{12}}{C_{11}}\right) A \quad (7)$$

where A is the amplitude of composition modulation and Cs are elastic constants. It is assumed that the value of A determined by this technique is the total amplitude characteristic of a three-dimensional array.

The nature of the strain amplitude–ageing time curve agrees with the theoretical predictions of Tsakalakos [25] and the experimental results of Ditchek and Schwartz [22] on Cu–Ni–Sn alloy. Similar results have also been obtained by Butler and Thomas [17] for their Cu–Ni–Fe alloy. Other results for comparison are not many as there are only a few experimental results where amplitudes have been measured. Results of Miyazaki *et al.* [26] on Cu–Ti deviate from the present trend. In that work the amplitude was found to increase even in the coarsening regime. However it has been argued [24] that the ageing temperature was above the spinodal and the apparent increase in amplitude may actually be representing increasing volume fraction of precipitates.

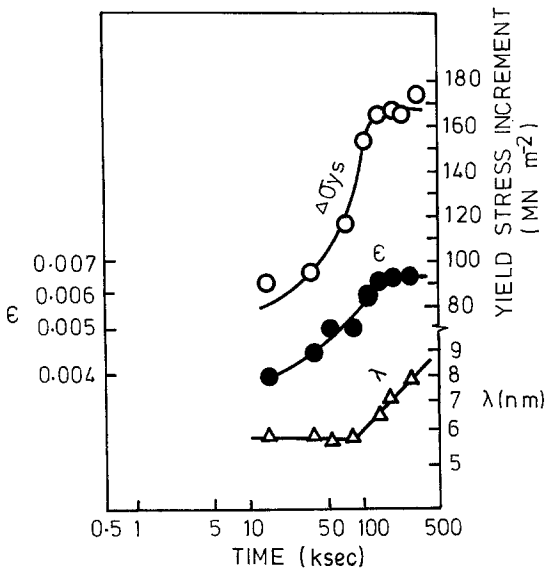

Figure 7 Variation of wavelength, strain amplitude and yield stress increment with ageing time at 773 K.

3.2. Microstructural studies

Transmission electron microscopic investigations were carried out in the quenched and aged conditions. Even though the presence of side bands in X-ray diffraction pattern is strong evidence, it is desirable to confirm that the alloy decomposes by the spinodal mechanism by independent evidence. Therefore the aim of these studies was not only to characterize the microstructure but to obtain independent evidence on the nature of transformation in these alloys. Specimens were studied after ageing at three temperatures 773, 823 and 1073 K.

Specimens aged for short duration at 773 K showed wavy dark and bright regions (Fig. 8a). When the specimen was aged for longer durations such as 400 ksec at 773 K the alignment of the precipitates could be seen very distinctly (Fig. 8b).

Fig. 9 shows the development of the modulated microstructure on ageing at 823 K. Within a short ageing period of 600 sec the particles were seen to be quite distinct. Fig. 9a shows the microstructure of a sample aged for 5.4 ksec at 823 K. The particles are still spherical but a tendency towards cuboidal shape could be noticed at higher magnifications. With further ageing the particles became fully cuboidal as shown in Fig. 9b for a sample aged for 54 ksec. After such long ageing periods the particles appeared to be clearly interconnected.

When the alloy was aged at 1073 K the coarsening was observed to progress rapidly (Fig. 10). During initial stages the particles were small, distinctly cuboidal and aligned in ⟨1 0 0⟩ direction. Precipitation occurred right up to the grain boundary. On further ageing cuboidal particles clustered together and coalesced into rods elongated in the ⟨1 0 0⟩ direction. On ageing for very long periods such as 360 ksec a network of dislocations was found to form around the particles, indicating complete loss of coherency.

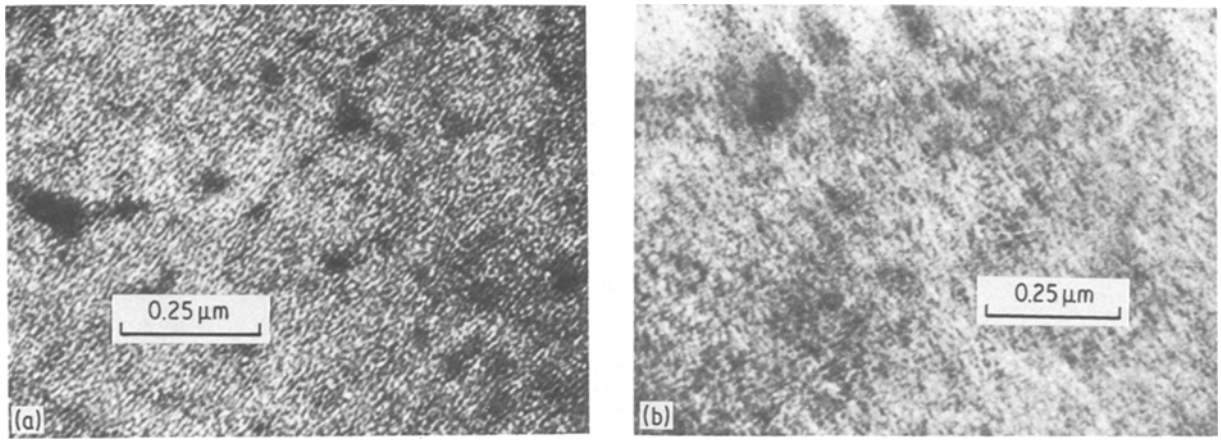

Figure 8 Microstructures after ageing at 773 K for (a) 54 ksec, (b) 400 ksec.

This sequence of morphological transformation: cuboids → rods → platelets can be explained in a qualitative manner using Kachathuryan's analysis [27].

The bright and dark areas in the microstructure were identified respectively as γ_1 and γ_2 phases [23]. No connectivity was observed between the γ_2 precipitates. After the analysis of Cahn [28], it is now generally agreed that connectivity should exist for precipitates with volume fractions greater than 0.2. Since the volume fraction γ_2 was estimated [23] to be less than 10%, no connectivity is expected between γ_2 particles.

Morphological features that characterize spinodal alloys are periodic array of precipitating phases, a high degree of interconnectivity between the precipitates, and absence of preferential precipitation at microstructural inhomogeneties such as grain boundaries and dislocations. No interconnectivity was observed amongst γ_2 particles for the reason already cited. Other features were observed in all the samples. Therefore it could be concluded that the alloy does undergo spinodal decomposition. Since the alloy was made to have a composition slightly outside the miscibility gap in the isothermal section at 1203 K of the Cu–Ni–Cr system it appears to suggest that this isothermal section needs to be redrawn.

3.3. Mechanical properties

Hardness was measured on samples isothermally aged for various durations of time in the temperature interval 773 to 1073 K and is shown in Fig. 11. Since a previous investigation [7] showed that kinetics of transformations was very slow at temperatures below 723 K, only ageing temperatures above 723 K were used in the present investigation. It was found that maximum hardness was attained on isothermally ageing in the temperature range 773 to 823 K. At higher ageing temperatures not only the time to reach the peak value decreased but also the peak value of the hardness itself was lower than that at lower temperatures. Ageing beyond the time needed to reach the peak hardness led to a drop in hardness. Fall in hardness with ageing time was extremely rapid at 923 and 1073 K. This suggests that the precipitates are coarsening very rapidly and lose coherency with the matrix quite early during the ageing process. At the isothermal ageing temperature of 1073 K, the peak hardness was reached within an ageing time of 2000 sec. Thereafter the hardness continued to drop rapidly. Microstructural investigations revealed, as already discussed, that the particles coalesced into rod morphology with the rods oriented in the ⟨1 0 0⟩ direction within 18 ksec of ageing time. The hardness

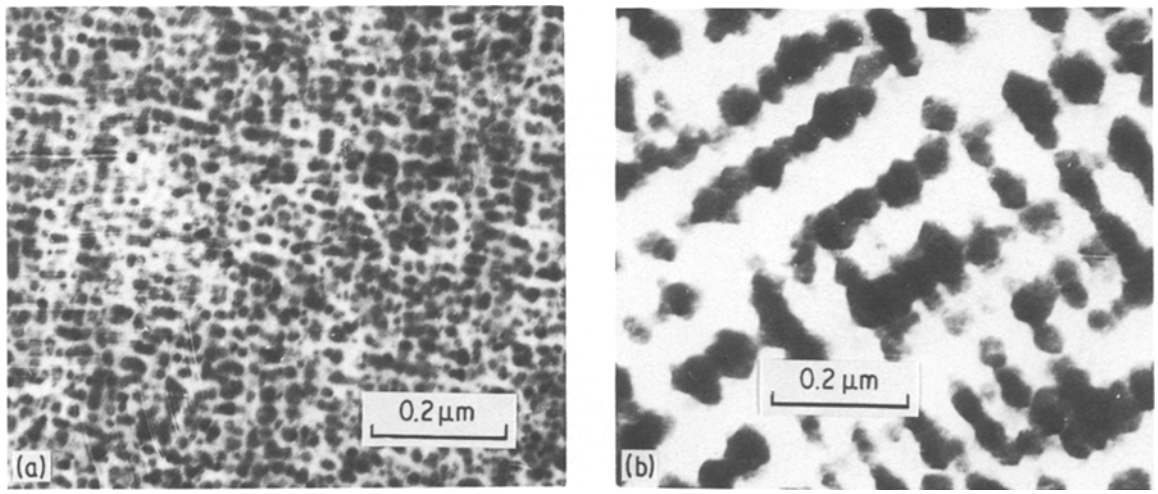

Figure 9 Microstructures after ageing at 823 K for (a) 5.4 ksec, (b) 36 ksec.

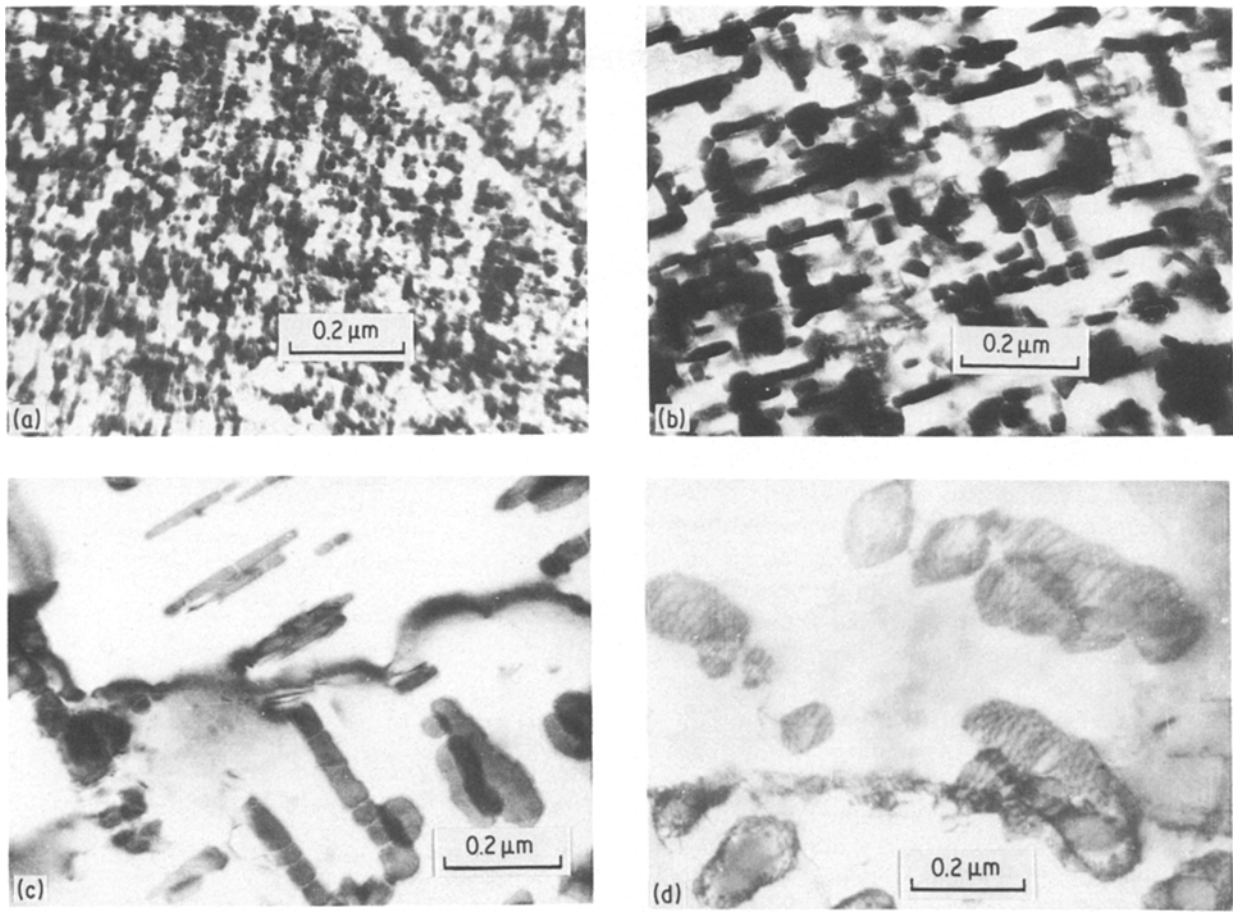

Figure 10 Microstructures after ageing at 1073 K for (a) 600 sec, (b) 18 ksec, (c) 36 ksec, and (d) 360 ksec.

at this stage is only 125 VPN as compared to the peak value of 148 VPN. Therefore the fall in hardness can be associated with the transformation in the microstructure from fine particles to rods. The appearance of the dislocations at the particle–matrix interface was noticed only much later.

Tensile tests revealed higher yield stress and lower elongation for aged specimens as compared to the as-quenched specimen. The variation in the increment in yield stress with ageing time at the isothermal ageing temperature of 773 K is shown in Fig. 7 which, as already discussed, also shows the variation in strain amplitude and wavelength of composition modulation with ageing time. From this, it can be seen that the

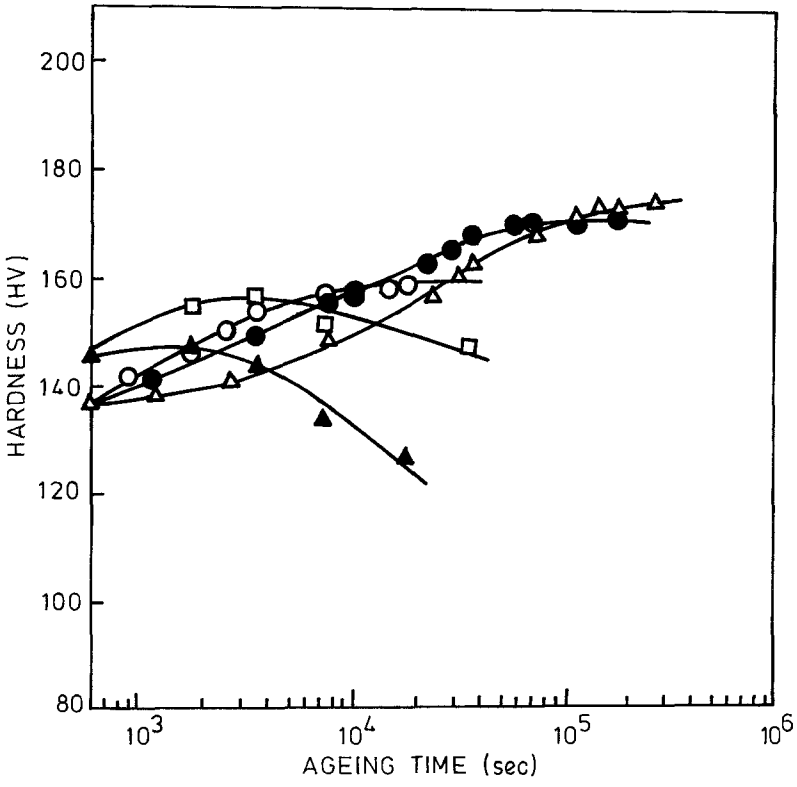

Figure 11 Variation of hardness with ageing time at various ageing temperatures. (▲) 1073 K; (□) 973 K; (○) 873 K; (●) 823 K; (△) 773 K.

yield stress increment and strain amplitude increased initially with ageing time but wavelength remained a constant. However, during later stages the wavelength started to increase but the yield stress increment and strain amplitude remained constant. These observations suggest that the variation in yield strength monotonically follows the variation of strain amplitude and is practically independent of the wavelength.

There are broadly two schools of thought on the mechanism of spinodal hardening. According to the first, the yield stress is dependent both on the strain amplitude and the wavelength of composition modulation. According to the second, the yield stress is dependent only on the strain amplitude and not on the wavelength. The models of Cahn [29], Gerold and Haberkorn [30], and that of Ditchek and Schwartz [24] fall under the first category whereas those of Dahlgren [31] and Kato *et al.* [32] fall under the second. From the observations in the present investigation the models which relate the strain amplitude alone to the yield stress appear valid.

4. Summary and conclusions

1. The alloy showed morphological features such as aligned precipitates and absence of preferential precipitation at microstructural inhomogeneities and presence of side bands in X-ray diffraction profiles confirming that it undergoes spinodal decomposition.

2. The variation of wavelength of composition modulation showed two distinct regimes. Initially the wavelength remained a constant followed by a coarsening regime when the wavelength increased with ageing time. During coarsening the wavelength was found to be proportional to cube root of time. The activation energy for this is about 270 kJ mol^{-1}.

3. The coherent spinodal temperature for the alloy is 946 K.

4. The variation of strain amplitude with ageing time is S shaped. It increases in the initial stage when the wavelength of composition modulation is a constant to reach a peak value and remains stationary thereafter while the wavelength increases continuously.

5. The yield stress increment due to spinodal hardening follows monotonically the variation in strain amplitude with ageing time. It is practically independent of the wavelength of composition modulation.

Acknowledgement

This work was carried out during the stay of one of the authors (P.P.R.) in the Department of Metallurgical Engineering, IIT Bombay under the Quality Improvement Programme of the Government of India. He, therefore, wishes to express his sincere thanks to the Principal, KREC, Surathkal, for granting him leave which made possible this stimulating stay at IIT, Bombay.

References

1. J. L. MEIJERING, G. W. RATHENAU, M. G. VAN DER STEEG and P. B. BRAUN, *J. Inst. Met.* **86** (1956) 158.
2. C. K. WU and G. THOMAS, *Metall. Trans. A* **8A** (1977) 1911.
3. A. CHOU, A. DATTA, G. H. MEIER and W. A. SOFFA, *J. Mater. Sci.* **13** (1978) 541.
4. D. BOWER, G. W. LORIMER, I. SAUNDERSON and P. WILKES, *Met. Technol.* **7** (1980) 120.
5. R. KNIGHTS and P. WILKES, *Metall. Trans.* **4** (1973) 2389.
6. A. J. ARDELL and R. B. NICHOLSON, *Acta Metall.* **14** (1966) 1295.
7. P. PRASAD RAO, B. K. AGRAWAL and A. M. RAO, *Trans. Indian Inst. Met.* **36** (1983) 264.
8. W. A. RACHINGER, *J. Sci. Inst.* **25** (1948) 254.
9. V. DANIEL and H. LIPSON, *Proc. R. Soc.* **A181** (1943) 368.
10. J. W. CAHN, *Trans. Met. Soc. AIME* **242** (1968) 166.
11. D. E. LAUGHLIN and J. W. CAHN, *Acta Metall.* **23** (1975) 329.
12. T. MIYAZAKI, S. TAKAGISHI, H. MORI and T. KOZAKARI, *ibid.* **28** (1980) 1143.
13. R. J. LIVAK and G. THOMAS, *ibid.* **19** (1971) 497.
14. J. E. HILLIARD, in "Phase Transformations", edited by H. I. Aaronson (American Society for Metals, Metals Park, 1970) p. 497.
15. I. M. LIFSHITZ and V. V. SLYOZOV, *J. Phys. Chem. Solids* **19** (1961) 35.
16. C. WAGNER, *Z. Elektrochem.* **65** (1961) 581.
17. E. P. BUTLER and G. THOMAS, *Acta Metall.* **18** (1970) 347.
18. T. MIYAZAKI, T. SHINOZAWA, H. MURAYAMA and H. MORI, *Trans. Jpn. Inst. Met.* **17** (1976) 181.
19. C. J. SMITHELS, in "Metals Reference Book" (Butterworths, London, 1976).
20. R. I. SAUNDERSON, P. WILKES and G. W. LORIMER, *Acta Metall.* **26** (1978) 1357.
21. R. W. CARPENTER, *ibid.* **15** (1967) 1567.
22. B. DITCHEK and L. H. SCHWARTZ, *ibid.* **28** (1980) 807.
23. P. PRASAD RAO, PhD thesis, Indian Institute of Technology (1983).
24. B. DITCHEK and L. H. SCHWARTZ, *Ann. Rev. Mater. Sci.* **9** (1979) 219.
25. T. TSAKALAKOS, PhD thesis, Northwestern University (1977).
26. T. MIYAZAKI, E. YAJIMA and H. SUGA, *Trans. Jpn. Inst. Met.* **12** (1971) 119.
27. A. G. KATCHATHURYAN, *Phys. Status Solidi* **35** (1969) 119.
28. J. W. CAHN, *J. Chem. Phys.* **42** (1965) 93.
29. *Idem, Acta Metall.* **11** (1963) 1275.
30. V. GEROLD and H. HABERKORN, *Phys. Status Solidi* **16** (1966) 675.
31. S. D. DAHLGREN, *Metall. Trans. A* **7A** (1976) 1661.
32. M. KATO, T. MORI and L. H. SCHWARTZ, *Acta Metall.* **28** (1980) 285.

Received 5 March 1984
and accepted 29 November 1985